Available online at www.sciencedirect.com
ScienceDirect
Journal of Sound and Vibration 314 (2008) 803–820
JOURNAL OF SOUND AND VIBRATION
www.elsevier.com/locate/jsvi

Exact solution of stable periodic one contact per N cycles motion of a damped linear oscillator contacting a unilateral elastic stop

C.N. Bapat*

Mechanical Engineering Department, The City College of New York, Convent Avenue at 138 West, New York 10031, USA

Received 14 December 2006; received in revised form 2 January 2008; accepted 9 January 2008
Handling Editor: Bolton
Available online 20 February 2008

Abstract

An exact closed-form solution is developed for a damped single-degree-of-freedom oscillator contacting a unilateral stop once per N cycles of external sinusoidal force. It also includes the effect of a bias force. This solution was obtained by using two different displacement and velocity expressions for a two-region piecewise linear oscillator, continuity of displacement and velocity at the boundary of the two regions, and periodicity conditions. Contact duration is assumed as known and four simultaneous equations in four unknowns are solved exactly. The four unknowns are the amplitude of the sinusoidal force, phase angle of the assumed first contact, entry velocity, and exit velocity of mass. The stability of motion is checked using the closed-form expressions of elements of a 2×2 stability governing matrix. These elements are obtained by considering only first-order perturbations in periodic motion. Theoretical predictions based on exact solution agree with previous results and with results obtained using a numerical simulation approach. The relationships are studied in detail between input parameters (such as amplitude of external force, frequency of external force, bias force, gap, spring stiffness and damping constants) and output parameters (such as contact duration, phase angle at contact, entry velocity, exit velocity, maximum displacement and minimum displacement).

1. Introduction

In the last few decades, a single-degree-of-freedom impact oscillator contacting stops has been widely used as a first approximation to study the behavior of machines used in pile driving, compacting, crushing, riveting, rock drilling, impact printing, marine structures and in contacts between baffle plates and tubes in heat exchangers used in the power, chemical and nuclear industries [1–4]. Interested readers should refer to these articles for additional information. The author is aware that extremely complex motions exist in these systems and extensive research has been undertaken using approximate methods such as describing functions, harmonic and incremental harmonic balance, stochastic linearization, approach of smoothening functions, finite elements in time, numerical simulation and mapping dynamics, and physical experiments. However, only articles related to closed-form solutions of periodic motions where the mass contacts the elastic stop once per

*Tel.: +1 212 650 5214.
E-mail address: bapat@ccny.cuny.edu

0022-460X/$ - see front matter © 2008 Elsevier Ltd. All rights reserved.
doi:10.1016/j.jsv.2008.01.024

Nomenclature

A_1	displacement amplitude, mm, $F/[(K_1-M\Omega^2)+(C_1\Omega)^2)]^{1/2}$
A_2	displacement amplitude, mm, $F/[(K_1+K_2-M\Omega^2)+\{(C_1+C_2)\Omega\}^2]^{1/2}$
C_1	viscous damping constant of primary system, N s/mm
C_2	viscous damping constant of stop, N s/mm
d	gap between mass and stop, mm
F	amplitude of sinusoidal force, N
K_1	stiffness of primary system, N/mm
K_2	stiffness of stop, N/mm
M	mass of primary system, kg
N	integer number of cycles per contact
P_2	stability matrix in region 2
P_1	stability matrix in region 1
r_1	frequency ratio (Ω/ω_1), non-dimensional
r_2	frequency ratio (Ω/ω_2), non-dimensional
t	time elapsed after the first contact, s
$X_1(t)$	absolute displacement of mass in region 1, mm
X_1	absolute displacement of mass at time 1, $X_1 = X_3 = d$, mm
$X_2(t)$	absolute displacement of mass in region 2, mm
X_2	absolute displacement of mass at time 2, equals d, mm
$X_{\max}$	maximum displacement of mass M, mm
$X_{\min}$	minimum displacement of mass M, mm
$Y_1(t)$	velocity of mass in region 1, mm/s
$Y_2(t)$	velocity of mass in region 2, mm/s
Y_i	velocity of mass at the ith contact, $i = 1$, 2 and 3 and $Y_3 = Y_1$, mm
ΔY_1	small perturbation in value Y_1 at first contact
α_1	phase angle between the displacement and force at the first contact, rad
$\Delta\alpha_1$	small perturbation in α_1 at first contact, rad
α_c	contact phase, rad
ξ_1	fraction of critical viscous damping, $C_1/2M\omega_1$
ξ_2	fraction of critical viscous damping, $(C_1+C_2)/2M\omega_2$
ω_1	undamped natural circular frequency in region one, rad/s
ω_2	undamped natural circular frequency in region two, rad/s
Ω	circular frequency of excitation, rad
$\mathrm{d}/\mathrm{d}t$	derivative with respect to time, t, superscript

N cycles of the external force are referenced in this work. These motions are important as stability regions can be quite large. When system parameters are outside stable regions of (1, N) motions, majority of complex periodic or chaotic motions occur.

Results obtained in this case need a solution of the resulting transcendental equations in unknown time durations between contacts and are solved numerically using a time consuming iteration approach. For this reason very few stability charts of such motions are available. Masri studied a simple oscillator and a beam contacting an elastic stop and solved the resulting nonlinear equations numerically [5]. A transcendental equation was obtained by Metallidis and Natsiavas [6] for a rod and a rigid mass contacting elastic stop under a sinusoidal and a bias force. Metallidis also solved these equations numerically. Ji also studied periodic motion of oscillator with saturation characteristics and developed nonlinear equations which were solved numerically [7,8]. Chicurel–Uziel studied mass oscillating against an elastic wall using periodizer function and used a symbolic mathematics package to obtain periodic motions [9]. Bapat studied an oscillator contacting a unilateral elastic stop once per cycle of applied force and developed four linear equations by assuming contact duration as a known. The resulting equations were solved using a digital computer [10]. However, explicit expressions of a stability matrix were not developed [10]. Instead the stability of motions was investigated using a numerical simulation approach using zero initial conditions. Obviously, those results were not conclusive.

Here, an approach is developed to obtain an exact closed-form solution for an oscillator contacting a single stop once per N cycles of an external sinusoidal force, and with a constant bias force. Additionally, explicit expressions of elements of stability matrix are also presented. Often pre-compression, d_c, and bias force are used to prevent impacts. However, during intense vibration the mass separates from the stop and impacts do occur. Theory developed here can be used to study such systems using $d = -d_c$. Theoretical predictions are

checked with results obtained using a numerical simulation approach and with previous results, and they agree. The interrelationships are investigated in detail between input parameters such as amplitude and frequency of sinusoidal force, bias force, gaps, spring stiffnesses, damping constants, and output parameters such as contact duration, phase angle at contact, entry velocity, exit velocity, and maximum/minimum displacement.

2. Theory

A model of an oscillator contacting an elastic stop at distance d is shown in Fig. 1(a) and it consists of a primary mass M, spring with stiffness K_1, and a damper with damping constant C_1. The system is excited by an external sinusoidal force $F\sin\Omega t$ and a bias force F_b. The elastic stop consists of a spring with stiffness K_2 and damper with damping constant C_2, and is located at distance d when $F = F_b = 0$. Negative or positive bias force shifts the static equilibrium position and, respectively, increases or reduces the gap d by F_b/K_1. The piecewise linear variation in spring and damping force is shown in Fig. 1(b) and (c), respectively. Fig. 2(a) shows one contact per three cycles motion and the important parameters such as phase angle of the assumed first contact, α_1, phase duration of joint motion, α_c, and velocities Y_1, and Y_2 of M as it enters and leaves region 2. The phase angle α_1 is angle Ωt between the displacement and the force at which the assumed first contact occurs, and the time is measured from this reference. The mass exits region 2 after time α_c/Ω with velocity Y_2. The phase plot of this motion is shown in Fig. 2(b). The contact phase α_c is assumed as a known. Equations relating four unknowns Y_1, Y_2, $A_1\cos\alpha_1$ and $A_1\sin\alpha_1$ are developed using exact solution of displacement and velocity between contacts and using continuity and periodicity conditions of motion. A_1 is the steady-state amplitude of oscillator only under external force $F\sin\Omega t$. It is assumed that stable periodic one contact per N cycles, i.e. (1, N), motion is established. Equations are developed and solved in a closed form in what follows.

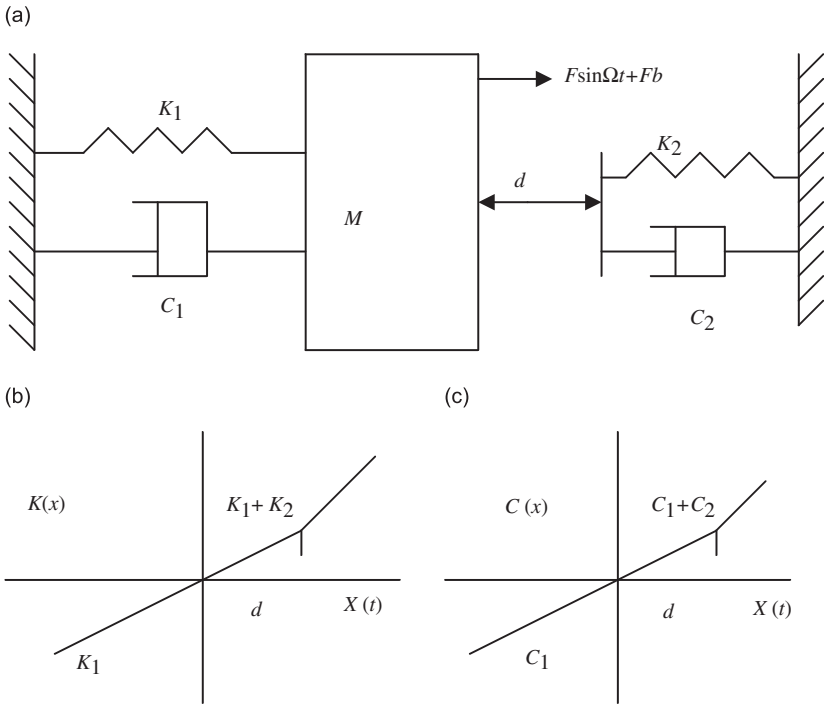

Fig. 1. (a) A single-degree-of freedom oscillator with elastic amplitude constraint under sinusoidal and bias force. The variations in spring force and damping force are shown in (b) and (c), respectively.

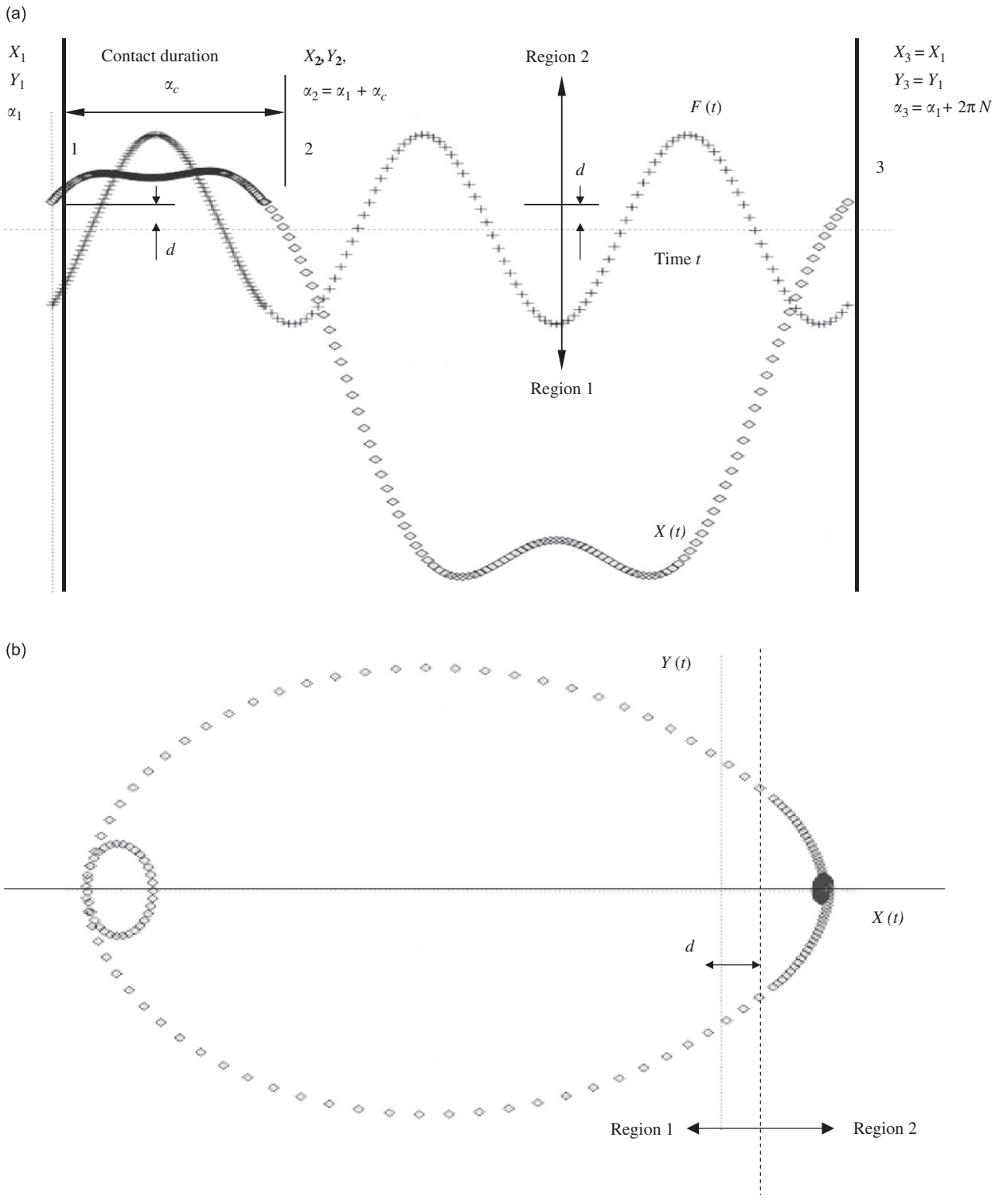

Fig. 2. (a) Displacement and force trace of one contact per three cycles, (1, 3) motion, with important parameters and (b) corresponding phase plane plot.

The differential equations of the motion of M between contacts in region 1 is given as

$$M\mathrm{d}^2X/\mathrm{d}^2t + C_1\,\mathrm{d}X/\mathrm{d}t + K_1X = F\sin(\Omega t) + F_b, \quad X(t)\leqslant d \tag{1}$$

and in region 2 as

$$M\,\mathrm{d}^2X/\mathrm{d}^2t + (C_1+C_2)\,\mathrm{d}X/\mathrm{d}t + (K_1+K_2)X = F\sin(\Omega t) + K_2d + F_b, \quad X(t)\geqslant d, \tag{2}$$

where X is the absolute displacement of M and is measured from the un-stretched spring position. When the mass is in region 2, it can be shown that between the assumed first and the second contact the displacement, $X_2(t)$, and velocity, $Y_2(t)$, is given as

$$\begin{aligned} X_2(t) = {} & \exp(-\zeta_2\omega_2(\Omega t-\alpha_1)/\Omega)[a_2\,\sin\{\eta_2\omega_2(\Omega t-\alpha_1)/\Omega\} + b_2\,\cos\{\eta_2\omega_2(\Omega t-\alpha_1)/\Omega\}] \\ & + A_2\,\sin(\Omega t-\psi_2) + F_2, \quad \alpha_1\leqslant\Omega t\leqslant\alpha_1+\alpha_c, \end{aligned} \tag{3}$$

$$\begin{aligned} Y_2(t) = {} & \exp(-\zeta_2\omega_2(\Omega t-\alpha_1)/\Omega)[a_2(\omega_2\{\eta_2\,\cos(\eta_2\omega_2(\Omega t-\alpha_1)/\Omega) - \zeta_2\,\sin(\eta_2\omega_2(\Omega t-\alpha_1)/\Omega)\} \\ & + b_2(\omega_2\{-\zeta_2\,\cos(\eta_2\omega_2(\Omega t-\alpha_1)/\Omega) - \eta_2\,\sin(\eta_2\omega_2(\Omega t-\alpha_1)/\Omega\}] + A_2\Omega\,\cos(\Omega t-\psi_2), \\ & \alpha_1\leqslant\Omega t\leqslant\alpha_1+\alpha_c. \end{aligned} \tag{4}$$

Expressions of all undefined variables in all equations are given in Appendix A. When mass is in region 1, displacement $X_1(t)$ and velocity $Y_1(t)$ between the second and the third contact is given as

$$\begin{aligned} X_1(t) = {} & \exp(-\zeta_1\omega_1(\Omega t-\alpha_1-\alpha_c)/\Omega)[a_1\,\sin\{\eta_1\omega_1(\Omega t-\alpha_1-\alpha_c)/\Omega\} + b_1\,\cos\{\eta_1\omega_1(\Omega t-\alpha_1-\alpha_c)/\Omega\}] \\ & + A_1\,\sin(\Omega t-\psi_1) + F_1, \quad \alpha_1+\alpha_c\leqslant\Omega t\leqslant 2\pi N+\alpha_1, \end{aligned} \tag{5}$$

$$\begin{aligned} Y_1(t) = {} & \exp(-\zeta_1\omega_1(\Omega t-\alpha_1-\alpha_c)/\Omega)[a_1\{\omega_1\{\eta_1\,\cos(\eta_1\omega_1(\Omega t-\alpha_1-\alpha_c)/\Omega) \\ & - \zeta_1\,\sin(\eta_1\omega_1(\Omega t-\alpha_1-\alpha_c)/\Omega)\} + b_1(\omega_1\{-\zeta_1\,\cos(\eta_1\omega_1(\Omega t-\alpha_1-\alpha_c)/\Omega) \\ & - \eta_1\,\sin(\eta_1\omega_1(\Omega t-\alpha_1-\alpha_c)/\Omega)] + A_1\Omega\,\cos(\Omega t-\psi_1), \quad \alpha_1+\alpha_c\leqslant\Omega t\leqslant 2\pi N+\alpha_1. \end{aligned} \tag{6}$$

As shown in Fig. 2(a), the displacement $X_2(t=\alpha_2/\Omega)=d$ and can be obtained from Eq. (3) after algebraic simplification as

$$d = X_2 = C_{12}a_2 + C_{22}b_2 + A_2\,\sin(\alpha_1+\alpha_c-\psi_2) + F_2. \tag{7}$$

Similarly, velocity Y_2 at the second contact can be obtained by substituting $\Omega t=\alpha_{1+}\alpha_c$ in Eq. (4) and is given as

$$Y_2 = C_{31}a_1 + C_{42}b_1 + A_2\Omega\,\cos(\alpha_1+\alpha_c-\psi_2). \tag{8}$$

The displacement and velocity of M at point 3 is obtained by substituting $\Omega t=(2\pi N+\alpha_1)$ in Eqs. (5) and (6), respectively. After simplification it can be written as

$$d = X_3 = C_{11}a_1 + C_{21}b_1 + A_1\,\sin(2\pi N+\alpha_1-\psi_1) + F_1, \tag{9}$$

$$Y_3 = Y_1 = C_{31}a_1 + C_{41}b_1 + A_1\Omega\,\sin(2\pi N+\alpha_1-\psi_1). \tag{10}$$

A careful examination of Eqs. (7)–(10) indicates that there are four simultaneous equations in six unknowns Y_1, Y_2, $A_1\cos\alpha_1$, $A_1\sin\alpha_1$, $A_2\cos\alpha_1$ and $A_2\sin\alpha_1$. All other variables can be calculated, as α_c is assumed to be known. However, the amplitude A_2 can be calculated in terms of A_1 as

$$A_2 = \lambda A_1,$$

where

$$\lambda = [(K_1-M\Omega^2)^2 + (C_1\Omega)^2]^{1/2}/[(K_1+K_2-M\Omega^2)^2 + ((C_1+C_2)\Omega)^2]^{1/2}. \tag{11}$$

Substituting A_2 in terms of A_1 in Eqs. (7) and (8) and Eqs. (9) and (10) results in four equations in four unknowns Y_1, Y_2, $A_1\sin\alpha_1$, and $A_1\cos\alpha_1$. After a lengthy algebraic simplification it can be shown that these four equations can be expressed as

$$W1R1 + W2R2 = B1, \tag{12a}$$

$$W3R1 + W4R2 = B2. \tag{12b}$$

Exact closed-form solution of Eq. (12a, b) can be obtained as

$$[R2] = [A_1 \cos \alpha_1, A_1 \sin \alpha_1] = [W1^{-1}W2^{-1} - W3^{-1}W4^{-1}]^{-1}[W1^{-1}B1 - W3^{-1}B2], \tag{13}$$

where

$$W1^{-1} = (\eta_2\omega_2/C_{12})\begin{bmatrix} 1 & 0 \\ C_{32}/\eta_2\omega_2 & -C_{12}/\eta_2\omega_2 \end{bmatrix},$$
$$W3^{-1} = (\eta_1\omega_1/C_{11})\begin{bmatrix} C_{31}/\eta_1\omega_1 & -C_{11}/\eta_1\omega_1 \\ 1 & 0 \end{bmatrix}. \tag{14}$$

Eq. (13) can be solved to obtain amplitude A_1, phase angle α_1 and external force F as

$$A_1 = [(A_1 \sin \alpha_1)^2 + (A_1 \cos \alpha_1)^2]^{1/2}, \quad \alpha_1 = \arctan[A_1 \sin \alpha_1/A_1 \cos \alpha_1] \tag{15a}$$

and

$$F = A_1[(K_1 - M\Omega^2)^2 + (C_1\Omega)^2]^{1/2}. \tag{15b}$$

The velocities Y_1 and Y_2 can be obtained by solving Eq. (12a) as

$$[R1] = [Y_1, Y_2]^{\mathrm{T}} = W1^{-1}[B1 - W2R2]. \tag{16}$$

Eqs. (16) and (17) are the closed-form solutions of A_1, α_1, F, Y_1 and Y_2.

For the given system parameters M, K_1, K_2, C_1, C_2, Ω and assumed contact duration α_c, C_{ij}, $i = 1$–4, $j = 1, 2$ and $W1$, $W2$, $W3$ and $W4$ remain the same and do not depend on d and F_b. However, a careful examination of the elements of $B1$ and $B2$ given by Eq. (A.4) indicates that $B1$ and $B2$ are proportional to the gap parameter $(dK_1 - F_b)$. Using these two facts in Eqs. (12), (15) and (16) indicates that $[R2] = [A_1\cos\alpha_1,\ A_1\sin\alpha_1]^{\mathrm{T}}$ and $[R1] = [Y_1,\ Y_2]^{\mathrm{T}}$ are proportional to the gap parameter $(dK_1 - F_b)$. When $d = F_b = 0$ or $K_1d - F_b = 0$ and the just mentioned proportional relationship results in $B1 = B2 = 0$. This leads to a trivial solution $Y_1 = Y_2 = A_1 = A_2 = F = 0$. The theory presented in this manuscript is not applicable for this special case. The case when $d = 0$ is quite interesting as contacts occur for all values of Ω when $F \neq 0$. However, intuitively, the responses of a system with a zero gap and that with a very small gap may be quite close. Theoretical results obtained using a very small gap and those obtained using zero gap in a digital simulation approach are close, and this confirms the above conjecture. These results are presented in Section 3.

Eqs. (13), (14) and (16) indicate that when C_{11}, C_{12} and $W1^{-1}W2 - W3^{-1}W4$ are very small, matrices $W1$, $W3$ and $[W1^{-1}W2 - W3^{-1}W4]^{-1}$ become nearly singular. In such instances it is advisable to further investigate using a digital simulation approach to confirm theoretical predictions. However, difficulties during inversion process can be predicted and avoided by checking the values of C_{12}, C_{11} and $W1^{-1}W2 - W3^{-1}W4$. This fact is used to indicate a problem and to avoid overflow in the computer program. Additionally, if an exceedingly large force is predicted then it is advisable to check the results using a digital simulation approach. However, such situations are expected to be rare and are not encountered in this investigation.

There are other physical requirements for motions to be viable, and one such requirement is that the amplitude $A_1 + F_b/K_1$ must be greater than the gap d

$$A_1 + F_b/K_1 > d. \tag{17}$$

Eq. (17) controls the frequency range of vibro-contact motion. Additionally, displacement must remain in regions 2 between the time interval 0–t_2 and in region 1 between the time interval t_2–t_3, respectively:

$$X_2(t) > d, \quad 0 \leqslant t \leqslant t_2, \quad X_1(t) < d, \quad t_2 \leqslant t \leqslant t_3. \tag{18a, b}$$

Also, the velocity of mass M as it enters region 2 must be positive, and as it leaves region 2 must be negative

$$Y_1 = Y_3 > 0, \quad Y_2 < 0. \tag{19}$$

Solutions not satisfying Eqs. (17)–(19) are rejected. However, violation of the displacement conditions Eqs. (18a, b) indicates that more than one contact occurs within the considered time interval. This fact can be

used to obtain end point of the assumed type of periodic motion. A majority of complex motions occurs when parameters are outside the stability regions of (1, N) motions. However, overlapping of (1, N) motions and other complex motions may occur in small regions, and some examples are presented in Section 3.

Periodic motions are further classified as stable and unstable. The stability of motion is investigated by perturbing motion. The elements of the 2×2 stability matrix P_2, are obtained by substituting $\alpha_1+\Delta\alpha_1$, $Y_1+\Delta Y_1$, $\alpha_2+\Delta\alpha_2$ and $Y_2+\Delta Y_2$ for α_1, Y_1, α_2 and Y_2 in Eqs. (7)–(10) and in expressions of a_2, b_2, C_{12}, C_{22}, C_{32}, C_{42} given in Appendix A. Expanding all terms of these equations and neglecting second-order terms, the relations between the above-mentioned perturbations can be expressed as [10]

$$\begin{bmatrix}\Delta\alpha_1\\ \Delta Y_2\end{bmatrix}=\begin{bmatrix}P_2(1,1) & P_2(1,2)\\ P_2(2,1) & P_2(2,2)\end{bmatrix}\begin{bmatrix}\Delta\alpha_1\\ \Delta Y_1\end{bmatrix}. \tag{20}$$

Following similar procedure, the perturbation matrix P_1 can be obtained when mass M is in region 1 during the time interval $t_2\leqslant t\leqslant t_3$. P_1 relates $\Delta\alpha_3$ and ΔY_3 to $\Delta\alpha_2$ and ΔY_2 and is given as

$$\begin{bmatrix}\Delta\alpha_2\\ \Delta Y_2\end{bmatrix}=\begin{bmatrix}P_1(1,1) & P_1(1,2)\\ P_1(2,1) & P_1(2,2)\end{bmatrix}\begin{bmatrix}\Delta\alpha_2\\ \Delta Y_2\end{bmatrix}. \tag{21}$$

The 2×2 total stability matrix P_T which relates perturbation at contact 3 to those at contact 1 is expressed as

$$P_T=P_1P_2. \tag{22}$$

Periodic motion is asymptotically stable if and only if all eigenvalues of matrix P_T lie within the unit circle in the complex plane. Two eigenvalues of P_T are given as

$$\lambda_{1,2}=0.5[P_T(1,1)+P_T(2,2)]\pm 0.5[\{P_T(1,1)+P_T(2,2)\}^2-4\{P_T(1,1)P_T(2,2)-P_T(1,2)P_T(2,1)\}]^2. \tag{23}$$

For stability

$$\text{abs}(\lambda_1)<1 \text{ and } \text{abs}(\lambda_2)<1. \tag{24}$$

A numerical simulation approach is also used to validate the theoretical results obtained using Eqs. (13)–(16) and to investigate other periodic and non-periodic motions. The numerical simulation program is developed using a combined linear interpolation, bisection, and constant time step approaches. The complete time history of motion is obtained using zero initial displacement $X(0)=0$ and velocity $Y(0)=0$ unless stated otherwise. The next contact instant t_2 is obtained by iteratively solving Eqs. (7) or (9), and computations are terminated when $\text{abs}(X(t_2)-d)\leqslant 10^{-8}$. New initial conditions are obtained as $X_2=d$ and Y given by Eqs. (4) or (6), and this process is continued for a long time. All computations are performed using a double precision arithmetic to reduce round off errors in numerical calculations.

Theoretical predictions agree with previous theoretical results and also with results obtained using the numerical simulation approach and are presented in Section 3. The interrelations between frequency and amplitude of sinusoidal force, bias force, gap, two stiffnesses, contact duration, and damping constants and important output parameters such as velocity at contact, maximum and minimum displacements, etc., are studied and presented in what follows.

3. Results and discussion

Results are obtained using $K_1=M=d=1$, $C_1=0.01$, $C_2=0.1$, $K_2=25$ and $F_b=0$ unless stated otherwise. Theoretical results obtained using Eqs. (16) and (17) for (1, 1) motion with and without biased force, (1, 2) motion at large force level near the upper end of the stability region at $\Omega=4.1$, and (1, 4) motion with a large contact duration at $\Omega=6$ and $F=40$ are compared with results obtained using a numerical simulation approach. These results are presented in Table 1 and they all concur. Small differences exist between results presented in Table 1 as amplitude of force is assumed as a known in simulation approach and contact duration α_c is obtained as one of the outputs. However, in theoretical solution contact duration, α_c is

Table 1
A comparison of theoretical results with simulation results

Type of motion	Parameters		Exact solution		Simulation results	
			Input	Output	Input	Output
(1, 1) stable	$C_1 = 0.01$	F		0.10002	0.1000	
	$\Omega = 1.0$	α_c	0.4372			0.4372
		α_1		1.4598		1.4596
		X_{max}, X_{min}		1.0440, −1.0565		1.0439, −1.0563
		Y_1, Y_2		0.3634, −03569		0.3634, −0.3568
(1, 1) stable	$C_1 = 0.01$	F		0.1000	0.1000	
Bias force	$\Omega = 1.0$	α_c	0.5029			0.5033
	$F_b = 0.5$	α_1		1.3766		1.3766
		X_{max}, X_{min}		1.0387, −0.0533		1.0387, −0.5330
		Y_1, Y_2		0.2679, −0.2619		0.2679, −0.2619
(1, 2) stable	$C_1 = 0.01$	F		30.0028	30.0	
	$\Omega = 4.1$	α_c	1.4454			1.4453
		α_1		3.9789		3.9788
		X_{max}, X_{min}		1.6917, −3.3710		1.6913, −3.3704
		Y_1, Y_2		7.1255, −7.0478		7.1254, −7.0479
(1, 4) stable	$C_1 = 0.01$	F		40.0000	40.0	
	$\Omega = 6$	α_c	6.4503654			6.4503654
		α_1		−1.6487		−1.6487
		X_{max}, X_{min}		2.1088, −11.0954		2.1073, −11.0947
		Y_1, Y_2		10.3973, −10.6512		10.3975, −10.6512

Please note that in the theoretical solution α_c is assumed as an input and F is one of the outputs.

assumed as an input, and required force F is one of the outputs. This leads to small differences in inputs and outputs as shown in Table 1. Displacement and force traces of these motions and corresponding phase plane plots are presented in Fig. 3(a)–(h). Results presented in row 1 of Table 1 also agree with results obtained previously by solving nonlinear coupled equations [5] and four linear simultaneous equations [10] for a case with $d = 1$. The motion corresponding to row four is interesting as mass completes one cycle in region 2 with large contact duration and then spends 3 cycles in region 1. A comparison of results shown in row 1 with $F_b = 0$ to those in row 2 with $F_b = 0.5$ indicates that bias force F_b increases contact duration from 0.4372 to 0.5029, reduces peak to peak amplitudes from 1.0440, −1.057 to 1.0387, −0.0533 and lowers contact velocities from 0.3634, −0.35687 to 0.2679 and −0.2619, respectively. This is clearly seen in Fig. 3(b) and (d). Comparing Fig. 3(b) to (d) also indicates that phase orbit in Fig. 3(d) shrinks significantly and mean position moves approximately F_b/K_1 in the direction of bias force. Generally, bias force is used to avoid impacts and to reduce displacement amplitude and contact velocities, and present results confirm this. However, bias force also increases contact force and contact duration, and may have adverse effect on wear rate due to increase in both parameters.

The important advantage of an exact solution as compared to the simulation approach is that exact results are obtained nearly instantaneously. Exact approach requires fixed number of calculations. As opposed to that, the simulation approach generally takes a long time to reach the steady-state motion due to slow convergence of the periodic motion. The time history in the form of a phase plane plot obtained using a digital simulation approach is shown in Fig. 4(a). It consists of an initial high amplitude response and eventual steady-state response obtained after nearly 1000 contacts. An exact solution for this case, which takes negligible computation time, is shown in Fig. 4(b) and is identical to the steady-state motion shown in Fig. 4(a). This clearly shows the advantage of an exact approach. The effects of various parameters on periodic motions are considered next.

The variation of amplitude of external force F as a function of contact duration α_c and input frequency Ω during (1, 1) motion is shown in Fig. 5(a) when $0 < \alpha_c < 0.4$ and in Fig. 5(b) when $0.4 < \alpha_c < 1.0$. This figure is

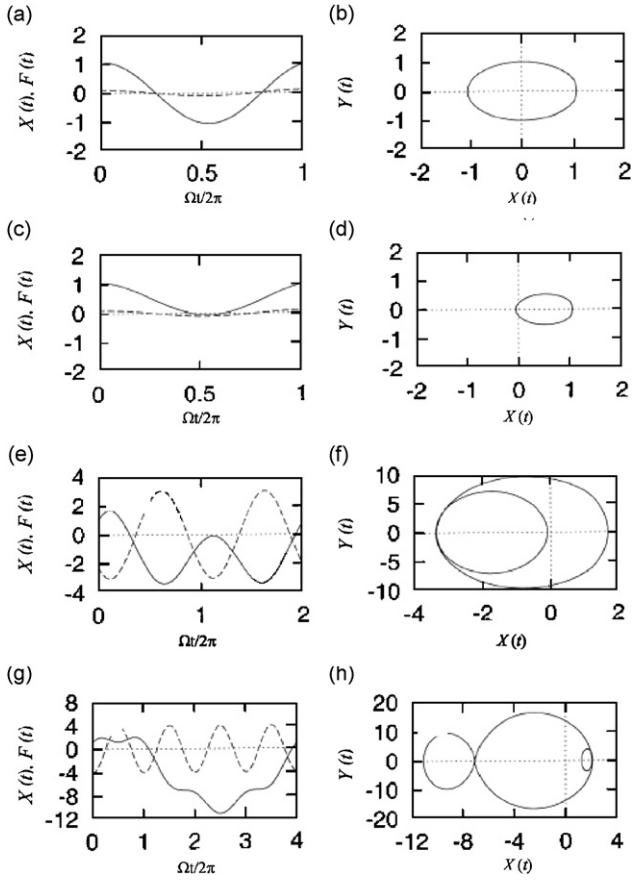

Fig. 3. Displacement and force traces of periodic motions presented in Table 1: (a) (1, 1) motion without bias force; (c) (1, 1) motion with bias force; (e) (1, 2) motion shown with $F/10$ and (g) (1, 4) motion with $F/10$. Corresponding phase plane plots are presented in (b), (d), (f) and (h), respectively. Force $F(t)$ (_ _ _) and displacement $X(t)$ (——).

obtained by increasing α_c by 0.001 in the range of 0–1. Gaps in α_c versus F curves indicate that for the ranges of values of α_c stable (1, 1) motion does not occur at the considered frequencies. As an example at $\Omega = 0.8$, (1, 1) motion occurs only when α_c was within $0.001 < \alpha_c < 0.065$ and $0.460 < \alpha_c < 0.522$. This behavior is quite common and indicates that stability diagrams drawn using Ω and α_c may have holes in some regions. Fig. 5(a) shows that at small contact duration, the required force increases very slowly with increasing contact duration. However, F changes in a nonlinear fashion over a large range of contact duration α_c. This response looks like that of a hardening spring and is clearly seen in Fig. 5(b). Fig. 5(b) also indicates that if stable (1,1) motion can occur at the same force level but at different excitation frequencies, then contact duration increases with the excitation frequency. These curves in Fig. 5(b) become nearly vertical near the higher value of α_c. Hence, cases in this vertical range are used to check the validity of theoretical predictions and to rule out the possibility of numerical underflow or overflow due to matrix inversion required in Eqs. (13) and (16). As an example at $\Omega = 1.1$ and $\alpha_c = 0.737$ and 0.738 the predicted values of F are 18.2193 and 22.5755, respectively. The slope of this curve in this range is quite high and approximately equals 4346.2. Detailed investigation predicted that (1, 1) motion is stable up to $\alpha_c = 0.738099$ and corresponding $F = 23.1138$. When $F \geqslant 23.1138$, (1, 1) motion is unstable. Hence, simulation results were obtained using $F = 22.5755$, $\Omega = 1.1$ and special initial conditions, $X(0) = 0$ and $Y(0) = -25$, which are close to periodic point of (1, 1) motion. This force is close to the higher end of the force range but is within the stability zone. Simulation confirmed the theoretical predictions that when $F = 22.5755$ stable (1, 1) motion occurs. Simulation results were also obtained using value of $F = 29.5304$ at input frequency $\Omega = 1.1$. This point is outside the stability range of (1, 1) motion. Simulation results confirmed the theoretical prediction, as at this force level three contacts/two cycles motion occurs.

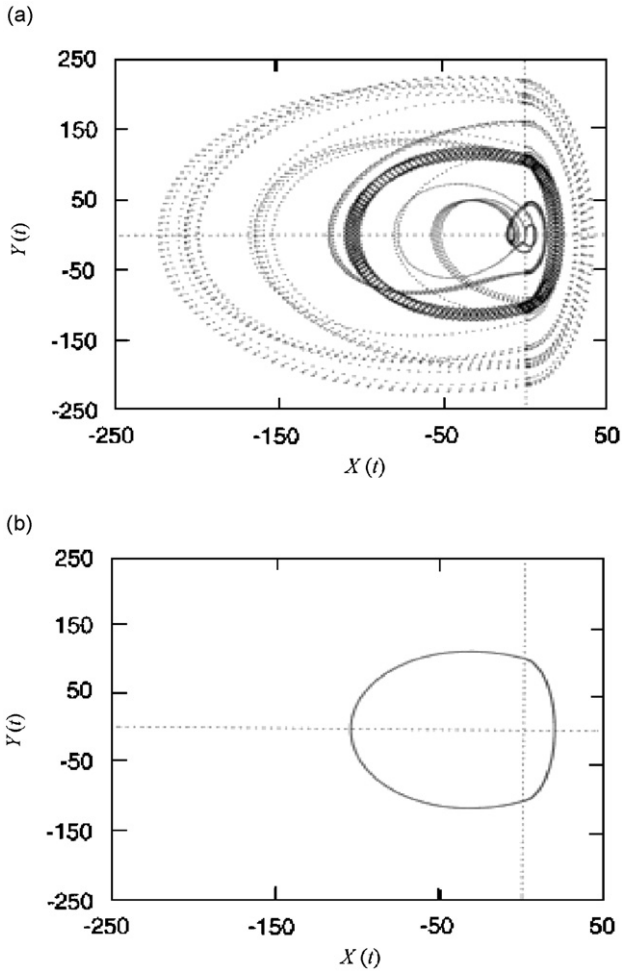

Fig. 4. (a) Numerical simulation results of initial transient (. . . . .), and final steady-state motion ($\diamond\diamond\diamond\diamond\diamond\diamond$), at $F = 80$, $\Omega = 2.0$ with $X(0) = Y(0) = 0$ and (b) corresponding theoretical solution.

Simple stable periodic motions are generally preferred as they are easy to study and operation is more uniform compared to other complex motions. The theory developed here can be used to obtain (1, N) motions in practice using initial condition $X(0) = X_{\min}$, where $Y(0) \approx 0$ and the phase angle Φ is given by $\sin(\Phi) = F(\text{at } X_{\min})/F$. The numerical value of Φ can be obtained by plotting one cycle of theoretical solution and finding Φ at $X_{\min}$ or using a computer program when $X(t)$ reaches $X_{\min}$. This information can be used in practice to obtain particular (1, N) motion by stretching system to $X_{\min}$ and triggering system to start operation at phase angle Φ. It is found that a stable system started with these conditions settles quite fast and produces the required steady-state motion. The theoretical solution is used in finding these initial conditions and can be helpful as domains of attraction regions are very complex. This approach can be especially useful in overlapping stability regions [11]. These initial conditions are used in numerical simulations of motions in what follows.

Behavior in the resonant region is studied in detail as it is quite important. Stability diagrams are obtained by increasing Ω by 0.01 and α_c by 0.001, respectively, in the range of $\Omega = 0$–2.5 and $\alpha_c = 0$–1.5. Corresponding stability diagrams of (1, N) motions for $N = 1$–4 are presented in Fig. 6. Similar stability diagrams are obtained at a high-frequency range of $\Omega = 2.5$–10 and $\alpha_c = 0.0$–7.0 by increasing Ω by 0.05 and α_c by 0.05. The results are presented in Fig. 7. Figs. 6 and 7 indicate that stability regions are not continuous as (1, N) motions occur only for certain ranges of α_c as explained before. Actual stability regions are slightly larger than those given in Figs. 6 and 7 as Ω and α_c are increased in discrete increments. However, they are within the increments

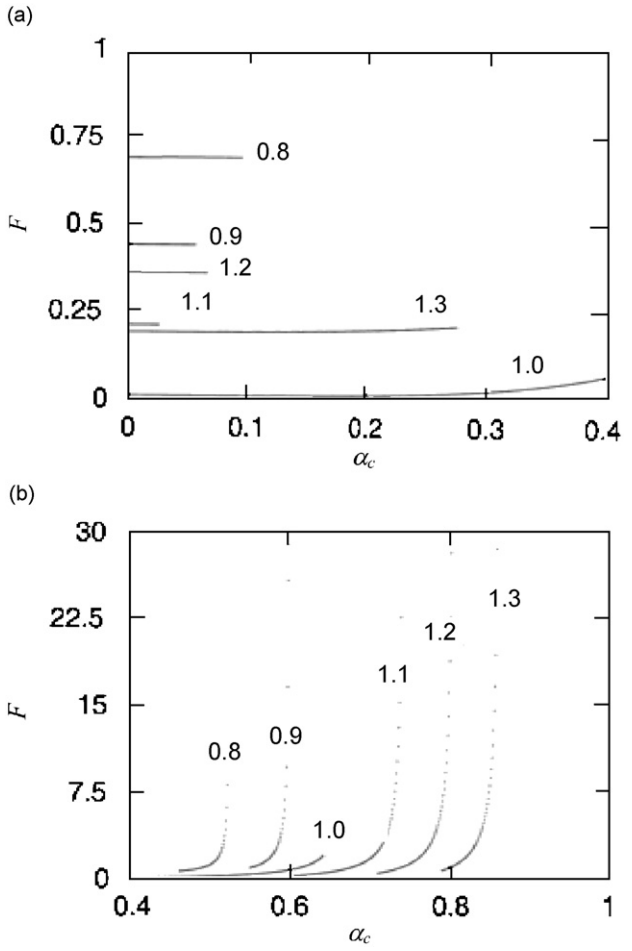

Fig. 5. Variation of input force F with contact duration α_c and input frequency Ω for (a) $0<\alpha_c\leqslant 0.4$ and (b) $0.4\leqslant\alpha_c\leqslant 1.0$.

in Ω and α_c mentioned above. Corresponding to (1, 1) motion shown in Figs. 6(a) and 7(a), only one diagram of F vs. Ω and α_c vs. F, for the entire range of $\Omega = 0$–10 and $\alpha_c = 0$–7, respectively, is shown in Fig. 8(a) and (b). It is clear from Fig. 8(b) that F vs. α_c curves are very steep near upper boundary of $\alpha_c \approx 1.3$ for high Ω. In such cases force is underestimated due to high slope near the end. Careful examination of Figs. 6 and 7 also shows that overlapping of stability regions occurs. This indicates that different motions can occur for the same system parameters, and the outcome depends on the initial conditions. As an example, at $\Omega = 10$, $d = 1$, $\alpha_c = 1.3$, $N = 1$ and $\Omega = 10$, $d = 1$, $\alpha_c = 6.54412$, $N = 6$ the theory predicted same $F = 1186.91$, but different entry and exit velocities of $Y_1 = 74.8799$, $Y_2 = -74.5803$ and $Y_1 = 699.5128$, $Y_2 = -814.6481$, respectively. This shows that overlapping stable (1, N) motions can be predicted theoretically. Simulation results were obtained using same $\Omega = 10$, $d = 1$, $F = 1186.91$ and using initial conditions $X(0) = -20.0$, $Y(0) = 0$, $\Phi = 1.58$ and $X(0) = 0.0$, $Y(0) = 0$ and $\Phi = 0$, respectively. Simulation results confirmed theoretical predictions. Velocities and contact durations were also identical to previously stated values obtained by theoretical predictions. Additionally, the example of Table 1—row 4 corresponds to the point $\Omega = 6$, $F = 40.0$ and $\alpha_c = 6.4550365$ and lies in the stability diagram of (1, 4) motion shown in Fig. 6(d). Generally, clearances in many mechanical systems are very small, and systems are operated well above the first resonance. Hence, investigation of these motions considered in Fig. 7 with large contact durations at high frequencies are important as they may lead to fretting wear in vibro-contact systems.

The motions corresponding to smaller values of α_c occur at small force levels and corresponding displacements amplitudes are slightly more than the gap d. These motions are similar to motions with grazing

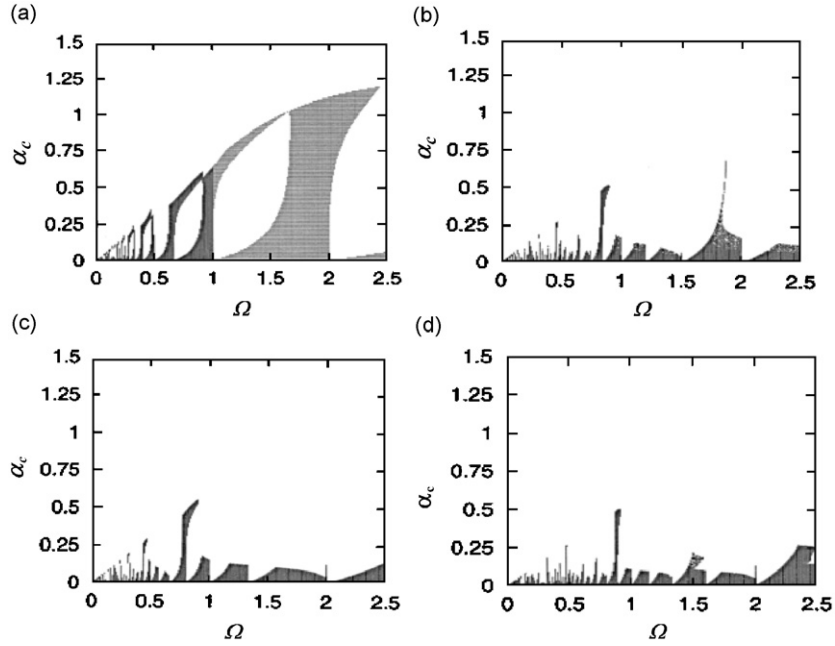

Fig. 6. Stability regions of (a) (1, 1); (b) (1, 2); (c) (1, 3) and (d) (1, 4) motions plotted with $\Omega = 0$–2.5 and $\alpha_c = 0$–1.5.

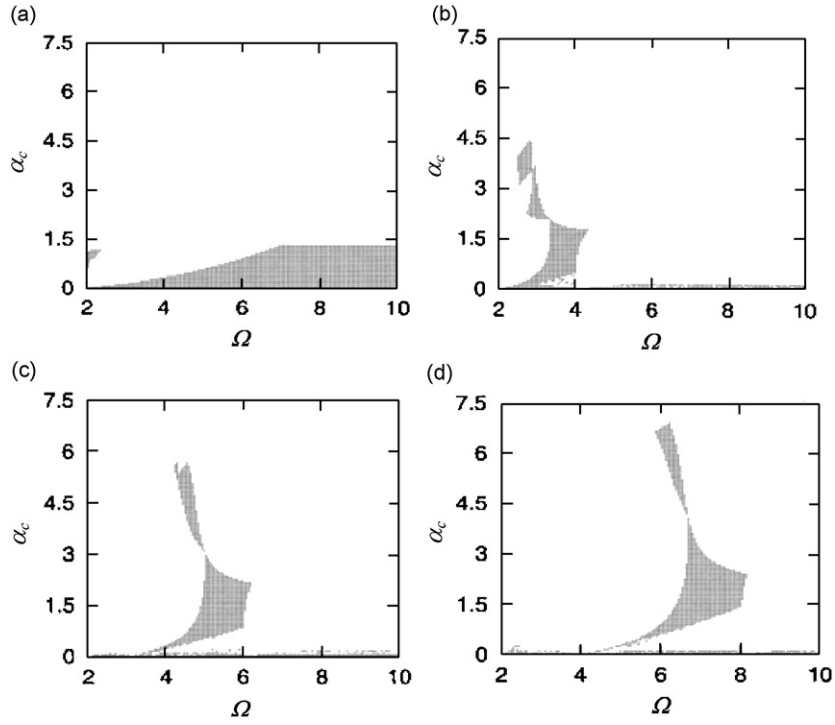

Fig. 7. Stability regions of (a) (1, 1); (b) (1, 2); (c) (1, 3) and (d) (1, 4) motions above primary resonance plotted with $\Omega = 2.0$–10 and $\alpha_c = 0$–7.5.

contacts [12,13]. A careful examination of all stability diagrams shown in Figs. 6 and 7 clearly show that stability regions of different (1, N) motions also overlap in this range. It is found that at the same force level, different (1, N) motions can occur with differing contact durations and in such cases the type of actual motion

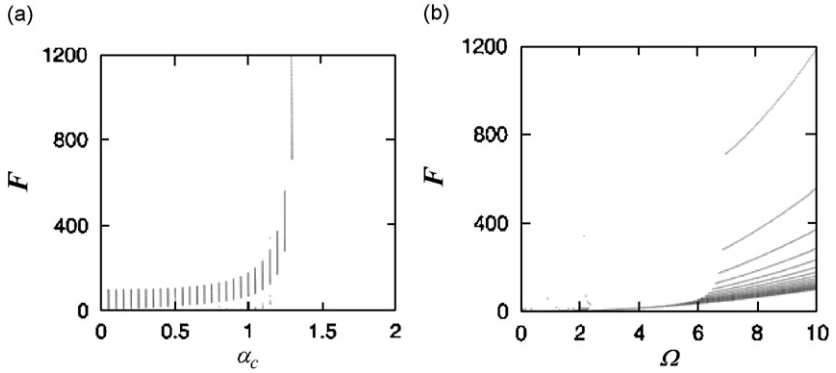

Fig. 8. The variation of (a) F vs. α_c and (b) F vs. Ω. Corresponding stability diagrams of (1, 1) stability regions for α_c vs. Ω are shown in Figs. 6(a) and 7(a).

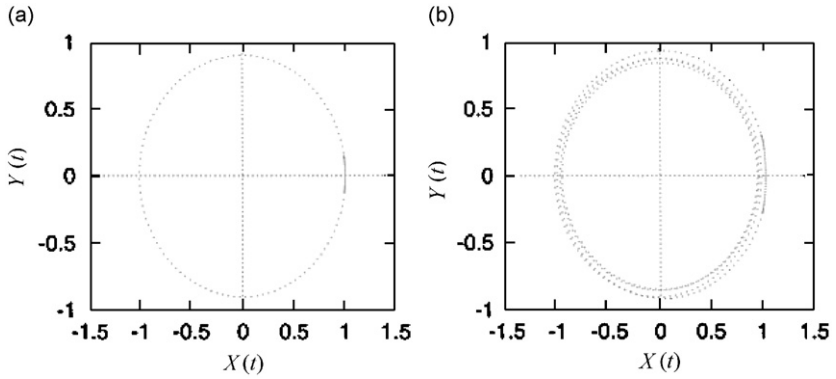

Fig. 9. Phase planes of overlapping of (1, N) regions at: (a) (1, 1) motion, $X(0) = -1$, $Y(0) = 0$, $\phi = 4.95$ and (b) (1, 4) motion, $X(0) = -1$, $Y(0) = 0$, $\phi = 3.26$ at $F = 0.20699$ and $\Omega = 0.9$. The presented results are obtained using simulation approach and they agree with theoretical results which are not shown.

depends on initial conditions. As an example, (1, 1) and (1, 4) motions overlap at $\Omega = 0.9$ when $F = 0.20699$. Results are obtained using a digital simulation approach using appropriate initial conditions, and are shown in Fig. 9(a) and (b). These results agree with theoretical predictions. Overlapping of more than two (1, N) type motions is also observed at other frequencies and force levels. To reduce propagation of errors during these weak interactions, the accuracy is increased during digital simulation by using condition $\text{abs}(X(t)-d) \leqslant 10^{-11}$ instead of $\text{abs}(X(t)-d) \leqslant 10^{-9}$. It is found that the system takes a long time to settle as contacts occur once per few cycles and the advantage of exact solution becomes quite clear. Very complex behavior of systems during grazing regions can be partially explained by overlapping of simple periodic motions as well as overlapping of simple motions with other complex motions. Simulation also indicates that settling times of grazing systems can be quite long. These observations may be important for experimental research of grazing motions since precisely controlling the amplitude of force and frequency is not an easy task. This partially explains the nonobservance of periodic vibro-contact motions in grazing regions.

Overlapping of (1, N) motions with other complex motions also occurs and two such examples are presented. When $F = 1.2$ and $\Omega = 0.45$ (1, 1) motion overlaps two contacts per cycle, i.e. (2, 1) motion, and is shown in Fig. 10(a)–(d). Also when $F = 22.57$ and $\Omega = 1.1$ (1, 1) motion overlaps 3 contacts per 2 cycles motion and these are shown in Fig. 10(e)–(h). These results are obtained using numerical approach with proper initial conditions. The theoretical predictions are identical to (1, 1) motions shown in Fig. 10(a) and (e).

Many times an elastic stop is introduced to limit displacement and velocity of vibrating systems. The effects of an elastic stop located at distance $d = 1$ on α_c, $2\pi-\alpha_c$, $X_{\max}/A_1$, $X_{\min}/A_1$, $Y_1/A_1\Omega$ and $Y_2/A_1\Omega$ is investigated. Results are obtained theoretically for stable (1, 1) motion using Eqs. (13)–(15). Contact duration

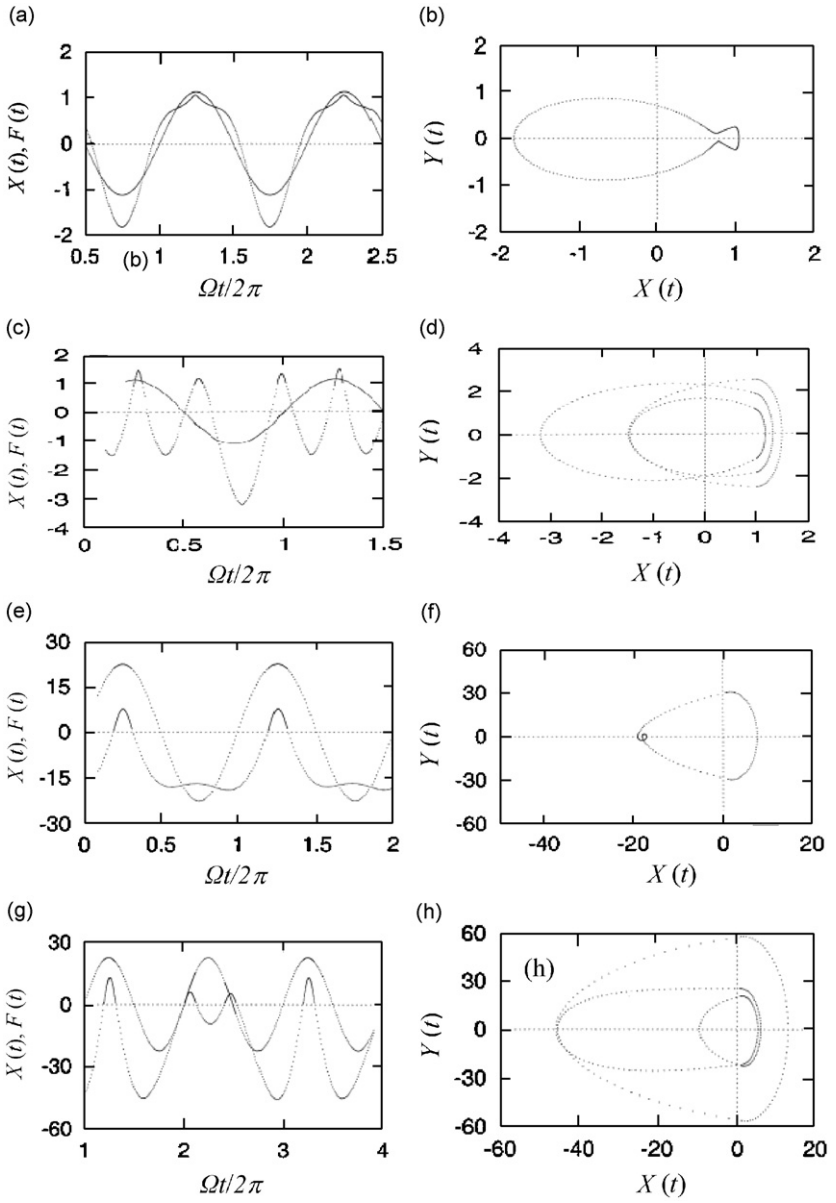

Fig. 10. Displacement and force traces and phase plane plots of overlapping of (1, 1) and (3, 1) motions at $\Omega = 0.45$, $F = 1.2$ are shown in (a), (c), (b) and (d), respectively. Similar plots of overlapping of (1, 1) and (3, 2) motions at $\Omega = 1.1$ and $F = 22.5655$ are shown in (e), (g), (f) and (h). These results are obtained using a simulation approach with initial conditions (a) $X(0) = -1.8$, $Y(0) = 0$, $\phi = 1.689$; (c) $X(0) = -1.0$, $Y(0) = 0$, $\phi = 0$; (e) $X(0) = -18$, $Y(0) = 0$, $\phi = 3.62$; and (g) $X(0) = 0$, $Y(0) = 0$, $\phi = 0$. Theoretical (1, 1) motions are exactly identical to those shown in (a) and (e).

α_c is increased very slowly and results are accepted when $0.999 \leqslant F \leqslant 1.001$ and are shown in Figs. 11(a), (c) and (e). Simulation results are obtained using $F = 1.0$, $X(0) = Y(0) = 0$ and are presented in Figs. 11(b), (d) and (f). Theoretical and simulation results agree with each other at all frequencies where (1, 1) motion occurs. In this case many other types of complex motions occur, especially below $\Omega = 0.7$, and are present in the simulation results. These figures also show that peaks of velocity and displacement occur at $\Omega \approx 0.21$, 0.41, 0.64, and 1.4. All values of non-dimensional variables above one represent amplification and below one represent attenuation. It can be seen that amplitude and velocity attenuation are achieved in the range around resonance of $\Omega = 0.63$–1.2 and outside this range amplification occurs. The minimum value of $X_{\max}/A_1$ and

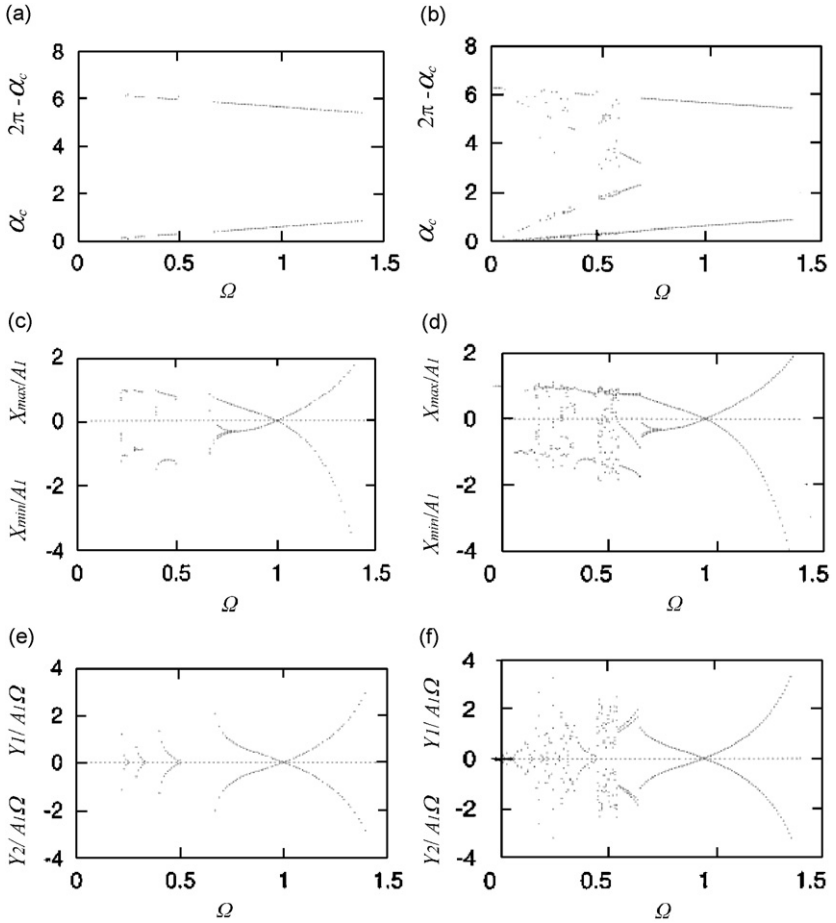

Fig. 11. Variation of α_c, $2\pi-\alpha_c$, $X_{\max}/A_1$, $X_{\min}/A_1$, $Y_1/A_1\Omega$ and $Y_2/A_1\Omega$ with Ω obtained using theory and simulation approach are presented in (a), (c), (e) and (b), (d), (f), respectively.

$X_{\min}/A_1$ occur at $\Omega = 1$ and these values increase more rapidly above one than below one and reach a maximum of approximately 4.5 at $\Omega \approx 1.41$. Contacts do not occur beyond $\Omega \approx 1.41$.

The conjecture that theoretical results obtained using a very small gap and results obtained using a simulation approach with a zero gap may be quite close to each other is further investigated in what follows. Theoretical results of (1, N) motions, $N = 1$, 2 and 3, are obtained using $d = 0.001$ and compared with those obtained using a simulation approach with $d = 0.0$. Other values of parameters, $C1 = 0.2$, $C_2 = 0.0$ and $K_2 = 4$ are chosen from Ref. [14] so that present results can be compared with previous results obtained using finite elements in time [14]. Theoretical results are obtained by increasing the contact duration very slowly, and results are accepted only when $0.999 \leqslant F \leqslant 1.001$ and are presented in Fig. 12(a) and (c). Simulation results are presented in Fig. 12(b) and (d). The present results agree amongst themselves and with those given in Fig. 2 of Ref. [14]. The system has local displacement peaks, during (1, 1), (1, 2) and (1, 3) motions, at $\Omega \approx 1.41$, 2.75 and 4.2, respectively. This behavior agrees with previous results [14]. It also confirms the above conjecture that if (1, N) motions occur then the differences between the results of a system with zero gap and those obtained theoretically using a very small gap will be minimum.

The results obtained indicate that contact duration decreases when spring stiffness increases and effect of damping constant C_2 is quite small [10]. However, positive bias force increases the contract duration. The velocity ratio also decreases with K_2; however, the effect of C_2 is more pronounced as the energy absorbed increases predominantly with C_2. This indicates that for a very large value of K_2 and with low damping C_2 it is reasonable to assume that contact interaction is close to instantaneous and can be modeled in the first approximation by a constant coefficient of restitution [15,16].

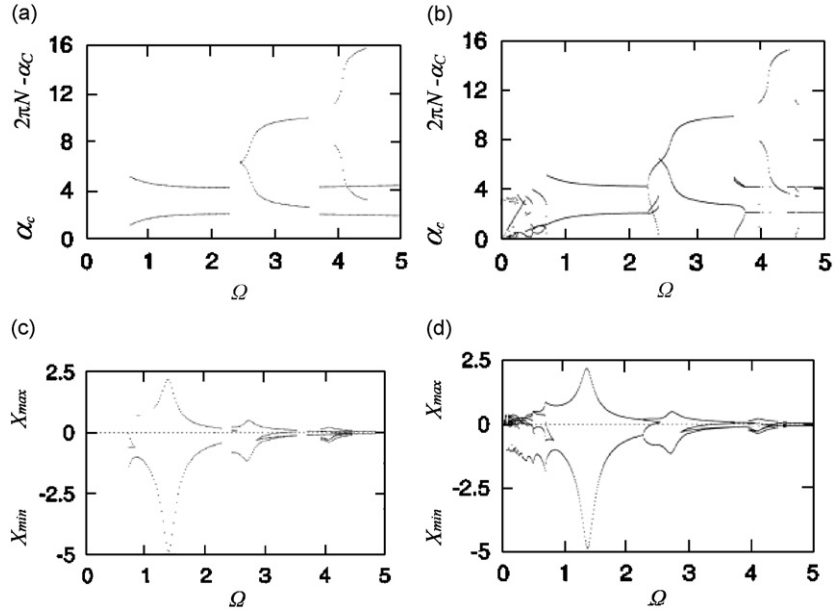

Fig. 12. Theoretical predictions of variation of α_c, $2\pi N-\alpha_c$, $X_{\max}$ and $X_{\min}$ with Ω obtained using $N = 1$, 2 and 3 are shown in (a) and (c). Results obtained using simulation approach are shown in (b) and (d). System parameters are: $F = 1.0$, $C_1 = 0.2$, $C_2 = 0.0$, $K_2 = 4$ and $d = 0.001$.

4. Conclusions

An exact theoretical approach is presented to study stable periodic one contact per N cycles of external force motion of a damped single-degree-of-freedom oscillator with piecewise linear variation in stiffness and damping properties. Contact duration is assumed as a known, and closed-form expressions of amplitude of the sinusoidal force, phase angle at impact, velocities at entry and exit are obtained. The stability of motion is studied by calculating eigenvalues of the 2×2 stability governing matrix. This matrix is obtained by perturbing periodic motion, and closed-form expressions for elements of the stability matrix are presented. Theoretical predictions agree with previous results and with results obtained using a numerical simulation approach. Relationships are studied in detail between input parameters, the amplitude and frequency of external force, bias force, gap, stiffness, damping constant and output parameters, namely contact duration, phase angle at contact, entry and exit velocities, maximum and minimum displacements.

Acknowledgements

The author acknowledges Mr. Milind Kunjir's help in formatting the figures. Also, support from the PSC-CUNY grant is acknowledged.

Appendix A

The undefined variables in the main text are given here. Variable required in Eqs. (3)–(6) are given as

$$\omega_2 = [(K_1 + K_2)/M)]^{1/2}, \quad \zeta_2 = (C_1 + C_2)/(2M\omega_2), \quad \eta_2 = (1 - \zeta_2^2)^{1/2}, \quad r_2 = \Omega/\omega_2,$$
$$\psi_2 = \tan^{-1}[2\zeta_2 r_2/(1 - r_2^2)], \quad A_2 = F/[(K_1 + K_2 - M\Omega^2)^2 + ((C_1 + C_2)\Omega)^2]^{1/2},$$
$$F_2 = (K_2 d + F_b)/(K_1 + K_2), \quad a_2 = (1/\eta_2)[(Y_1/\omega_2) - A_2 r_2 \cos(\alpha_1 - \psi_2) + \zeta_2 b_2],$$
$$b_2 = d - A_2 \sin(\alpha_1 - \psi_2) - F_2 \tag{A.1}$$

and

$$\omega_1 = (K_1/M)^{1/2}, \quad \zeta_1 = C_1/(2M\omega_1), \quad \eta_1 = (1-\zeta_1^2)^{1/2}, \quad r_1 = \Omega/\omega_1,$$
$$\psi_1 = \tan^{-1}[2\zeta_1 r_1/(1-r_1^2)], \quad A_1 = F/[(K_1 - M\Omega^2)^2 + (C_1\Omega)^2]^{1/2}, \quad F_1 = F_b/K_1,$$
$$a_1 = (1/\eta_1)[(Y_2/\omega_1) - A_1 r_1 \cos(\alpha_1 + \alpha_c - \psi_1) + \zeta_1 b_1], \quad b_1 = d - A_1 \sin(\alpha_1 + \alpha_c - \psi_1) - F_1. \tag{A.2}$$

Variable required in Eqs. (7)–(10) are given as

$$C_{12} = \exp(-\zeta_2\omega_2\alpha_c/\Omega)\sin(\eta_2\omega_2\alpha_c/\Omega), \quad C_{22} = \exp(-\zeta_2\omega_2\alpha_c/\Omega)\cos(\eta_2\omega_2\alpha_c/\Omega),$$
$$C_{32} = \omega_2(\eta_2 C_{22} - \zeta_2 C_{12}), \quad C_{42} = -\omega_2(\zeta_2 C_{22} + \eta_2 C_{12}),$$
$$C_{11} = \exp(-\zeta_1\omega_1 Z_1/\Omega)\sin(\eta_1\omega_1 Z_1/\Omega), \quad C_{21} = \exp(-\zeta_1\omega_1 Z_1/\Omega)\cos(\eta_1\omega_1 Z_1/\Omega),$$
$$C_{31} = \omega_1(\eta_1 C_{21} - \zeta_1 C_{11}), \quad C_{41} = -\omega_1(\zeta_1 C_{21} + \eta_1 C_{11}), \quad Z_1 = (2\pi N - \alpha_2). \tag{A.3}$$

The expressions of 2×1 matrices $R1$, $R2$, $B1$, and $B2$ and other variables required in Eqs. (12)–(14) are given as

$$R1 = [Y_1, Y_2]^{\mathrm{T}}, \quad R2 = [A_1\cos(\alpha_1),\ A_1\sin(\alpha_1)]^{\mathrm{T}},$$
$$B1(1) = (dK_1 - F_b)(1 - C_{12}\zeta_2/\eta_2 - C_{22})/(K_1 + K_2),$$
$$B1(2) = (dK_1 - F_b)(-C_{32}\zeta_2/\eta_2 - C_{42})/(K_1 + K_2),$$
$$B2(1) = (dK_1 - F_b)(1 - C_{11}\zeta_1/\eta_1 - C_{21})/K_1,$$
$$B2(2) = (dK1 - F_b)(-C_{31}\zeta_1/\eta_1 - C_{41})/K_1, \tag{A.4}$$

$$W1(1,1) = C_{12}/\eta_2\omega_2, \quad W1(1,2) = 0, \quad W1(2,1) = C_{32}/\eta_2\omega_2, \quad W1(2,2) = -1,$$
$$W2(1,1) = V1\cos\psi_2 - V2\sin\psi_2, \quad W2(1,2) = V1\sin\psi_2 + V2\cos\psi_2,$$
$$W2(2,1) = V3\cos\psi_2 - V4\sin\psi_2, \quad W2(2,2) = V3\sin\psi_2 + V4\cos\psi_2,$$
$$W3(1,1) = 0, \quad W3(1,2) = C_{11}/\eta_1\omega_1, \quad W3(2,1) = -1,\ W3(2,2) = C_{31}/\eta_1\omega_1,$$
$$W4(1,1) = V5\cos\psi_1 - V5\sin\psi_1, \quad W4(1,2) = V5\sin\psi_1 + V5\cos\psi_1,$$
$$W4(2,1) = V7\cos\psi_1 - V8\sin\psi_1, \quad W4(2,2) = V7\sin\psi_1 + V8\cos\psi_1 \tag{A.5}$$

and

$$V1 = \lambda(-C_{12}r_2/\eta_2 + \sin\alpha_c), \quad V2 = \lambda(-C_{12}\zeta_2/\eta_2 - C_{22} + \cos\alpha_c),$$
$$V3 = \lambda(-C_{32}r_2/\eta_2 + \Omega\cos\alpha_c), \quad V4 = \lambda(-C_{32}\zeta_2/\eta_2 - C_{42} - \Omega\sin\alpha_c),$$
$$V5 = C_{11}(-r_1\cos\alpha_c - \zeta_1\sin\alpha_c)/\eta_1 - C_{21}\sin\alpha_c,$$
$$V6 = C_{11}(r_1\sin\alpha_c - \zeta_1\cos\alpha_c)/\eta_1 - C_{21}\cos\alpha_c + 1,$$
$$V7 = C_{31}(-r_1\cos\alpha_c - \zeta_1\sin\alpha_c)/\eta_1 - C_{41}\sin\alpha_c + \Omega,$$
$$V8 = C_{31}(r_1\sin\alpha_c - \zeta_1\cos\alpha_c)/\eta_1 - C_{41}\cos\alpha_c. \tag{A.6}$$

Closed-form expressions of elements of the 2×2 matrices P_2 and P_1 are, respectively, given as

$$P_2(1,1) = [a_2 C_{32}/\Omega + b_2 C_{42}/\Omega - A_2 C_{12}\{r_2\sin(\alpha_1 - \psi_2) - \zeta_2\cos(\alpha_1 - \psi_2)\}/\eta_2 + A_2 C_{22}\cos(\alpha_1 - \psi_2)]/U_{12},$$
$$P_2(1,2) = -C_{12}/(\eta_2\omega_2 U_{12}), \quad P_2(2,1) = U_{22}P_2(1,1) + U_{32}, \quad P_2(2,2) = U_{22}P_2(1,2) + U_{42},$$
$$U_{12} = C_{32}a_2/\Omega + C_{42}b_2/\Omega + A_2\cos(\alpha_1 + \alpha_c - \psi_2),$$
$$U_{22} = a_2(\eta_2 C_{42} - \zeta_2 C_{32})/r_2 + b_2(-\eta_2 C_{32} - \zeta_2 C_{42})/r_2 - A_2\Omega\sin(\alpha_1 + \alpha_c - \psi_2),$$
$$U_{32} = -a_2(\eta_2 C_{42} - \zeta_2 C_{32})/r_2 - b_2(-\eta_2 C_{32} - \zeta_2 C_{42})/r_2 - A_2 C_{42}\cos(\alpha_1 - \psi_2) + A_2 C_{32}[r_2\sin(\alpha_1 - \psi_2) - \zeta_2\cos(\alpha_1 - \psi_2)]/\eta_2, \quad U_{42} = C_{32}/(\eta_2\omega_2), \tag{A.7}$$

$$
\begin{aligned}
P_1(1,1) &= [a_1C_{31}/\Omega + b_1C_{41}/\Omega - A_1C_{11}\{r_1\ \sin(\alpha_1+\alpha_c-\psi_1) - \zeta_1\ \cos(\alpha_1+\alpha_c-\psi_1)\}/\eta_1 \\
&\quad + A_1C_{21}\ \cos(\alpha_1+\alpha_c-\psi_1)]/U_{11}, \\
P_1(1,2) &= -C_{11}/(\eta_1\omega_1U_{11}), \quad P_1(2,1) = U_{21}P_1(1,1) + U_{31}, \quad P_1(2,2) = U_{21}P_1(1,2) + U_{41}, \\
U_{11} &= C_{31}a_1/\Omega + C_{41}b_1/\Omega + A_1\ \cos(\alpha_1-\psi_1), \\
U_{21} &= a_1(\eta_1C_{41} - \zeta_1C_{31})/r_1 + b_1(-\eta_1C_{31} - \zeta_1C_{41})/r_1 - A_1\Omega\ \sin(\alpha_1-\psi_1), \\
U_{31} &= -a_1(\eta_1C_{41} - \zeta_1C_{31})/r_1 - b_1(-\eta_1C_{31} - \zeta_1C_{41})/r_1 - A_1C_{31}\ \cos(\alpha_1+\alpha_c-\psi_1) \\
&\quad + A_1C_{31}[r_1\ \sin(\alpha_1+\alpha_c-\psi_1) - \zeta_1\ \cos(\alpha_1+\alpha_c-\psi_1)]/\eta_1, \quad U_{41} = C_{31}/(\eta_1\omega_1).
\end{aligned} \tag{A.8}
$$

References

[1] S. Natsiavas, Periodic response and stability of oscillators with symmetric trilinear restoring force, *Journal of Sound and Vibration* 134 (2) (1989) 315–331.

[2] S. Natsiavas, On the dynamics of oscillators with bi-linear damping and stiffness, *International Journal of Non-Linear Mechanics* 25 (5) (1990) 535–554.

[3] S. Natsiavas, Stability and bifurcation analysis for oscillators with motion limiting constraints, *Journal of Sound and Vibration* 141 (1) (1990) 97–102.

[4] M.S.T. de Freitas, R.L. Viana, C. Grebogi, Erosion of the safe basin for the transversal oscillations of a suspension bridge, *Chaos, Solitons & Fractals* 18 (4) (2003) 829–841.

[5] S.F. Masri, Analytical and experimental studies of a dynamic system with a gap, American Society of Mechanical Engineers, *Journal of Mechanical Design* 100 (3) (1978) 480–486.

[6] P. Metallidis, S. Natsiavas, Vibration of a continuous system with clearance and motion constraints, *International Journal of Non-Linear Mechanics* 35 (4) (2000) 675–690.

[7] J.C. Ji, Dynamics of a piecewise linear system subjected to a saturation constraint, *Journal of Sound and Vibration* 271 (4) (2004) 905–920.

[8] J.C. Ji, A.Y.T. Leung, Periodic and chaotic motions of a harmonically forced piecewise linear system, *International Journal of Mechanical Sciences* 46 (12) (2004) 807–1825.

[9] E. Chicurel-Uziel, Exact single equation, closed-form solution of vibrating systems with piecewise linear springs, *Journal of Sound and Vibration* 245 (2) (2001) 285–301.

[10] C.N. Bapat, Exact analysis of an oscillator hitting a stop, American Society of Mechanical Engineers, *Journal of Vibration, Acoustics, Stress and Reliability in Design* 107 (3) (1985) 347–350.

[11] C.N. Bapat, S. Sankar, N. Popplewell, Repeated impacts on a sinusoidal vibrating table reappraised, *Journal of Sound and Vibration* 108 (1) (1986) 99–115.

[12] A.P. Ivanov, Stabilization of an impact oscillator near grazing incidence owing to resonance, *Journal of Sound and Vibration* 162 (3) (1993) 562–565.

[13] A.B. Nordmark, Non-periodic motion caused by grazing incidence in an impact oscillator, *Journal of Sound and Vibration* 145 (2) (1991) 279–297.

[14] Y. Wang, Dynamics of asymmetric piecewise-linear/non-linear systems using finite elements in time, *Journal of Sound and Vibration* 185 (1) (1995) 155–170.

[15] S.W. Shaw, P.J. Holmes, A periodically forced piecewise linear oscillator, *Journal of Sound and Vibration* 90 (1) (1983) 115–129.

[16] C.N. Bapat, Periodic motions of an impact oscillator, *Journal of Sound and Vibration* 209 (1) (1998) 43–60.